JGR Oceans

RESEARCH ARTICLE
10.1029/2020JC016295

Key Points:
- Traditional and tailored climate indices are used to assess the predictability of extreme sea level variations
- Models developed in the frequency domain outperform traditional models in predicting extreme sea level variations
- Initialized decadal climate model simulations are used to assess the predictability of extreme sea level variations at decadal time scales

Supporting Information:
- Supporting Information S1

Correspondence to:
M. M. Rashid,
md.rashid@ucf.edu

Citation:
Rashid, M. M., & Wahl, T. (2020). Predictability of extreme sea level variations along the U.S. coastline. *Journal of Geophysical Research: Oceans*, *125*, e2020JC016295. https://doi.org/10.1029/2020JC016295

Received 4 APR 2020
Accepted 17 AUG 2020
Accepted article online 19 AUG 2020

Predictability of Extreme Sea Level Variations Along the U.S. Coastline

M. M. Rashid[1] and T. Wahl[1]

[1]Civil, Environmental, and Construction Engineering and National Center for Integrated Coastal Research, University of Central Florida, Orlando, FL, USA

Abstract Extreme sea level variability (excluding the effects of mean sea level (MSL) and long-period tidal cycles) at decadal to multidecadal time scales is significant along the U.S. coastlines and can modulate coastal flood risk in addition to long-term MSL rise. Therefore, understanding the climatic drivers and ultimately predicting these low-frequency variations are important. Extreme sea level indicators are used to represent the variations in 100-year return water levels, estimated with a nonstationary extreme value analysis. Here, we develop prediction models in the frequency domain. Extreme sea level indicators (response) and potential predictors (traditional climate indices, sea level pressure [SLP], or sea surface temperature [SST]) are decomposed into subseries corresponding to predefined frequencies using discrete wavelet transform (DWT), and regression models are formulated for each frequency separately. In the case of traditional climate indices, subseries of climate indices that provide the highest correlation with the corresponding subseries of indicators are used in the regression models, and original indicators are reconstructed by aggregating predicted subseries. Tailored climate indices are developed for each frequency band by averaging wavelet decomposed subseries of SLP or SST from grid locations where correlations with corresponding decomposed subseries of extreme sea level indicators are highest and robust. Models with wavelet filtered climate indices reproduce the variability and general trends of the indicators. The use of tailored indices further improves the model performance in predicting extreme sea level variations. Model performance in terms of Nash-Sutcliffe efficiency statistics varies from 0.54 to 0.93. Prediction of extreme sea level indicators using tailored indices derived from SLP and SST of initialized decadal climate model simulations is also tested to facilitate progress toward forecasting extreme sea level variations at decadal time scales.

Plain Language Summary Decadal to multidecadal variability of extreme sea levels is often omitted in coastal flood risk assessments, yet it can modulate flood risk in addition to long-term mean sea level rise, which is often considered as the only oceanographic driver for flood risk changes through time. In this study, we develop models to predict extreme sea level variations using traditional and tailored climate indices as predictors. Tailored climate indices are derived from gridded sea level pressure (SLP) and sea surface temperature (SST) to establish strong and robust relationships with extreme sea level variations. Models developed with traditional climate indices reproduce the overall extreme sea level variations, but prediction skill improves further with tailored climate indices. The results demonstrate the potential applicability of similar models to forecast extreme sea level variations at decadal time scales.

1. Introduction

Different drivers contributing to sea level variability along the coast such as mean sea level (MSL), storm surges, and tides exhibit significant fluctuations at different time scales, from seasonal to decadal. While long-term changes of MSL and its contributions to sea level variability have been extensively investigated (Carson et al., 2017; Dangendorf, Calafat, et al., 2014; Kopp et al., 2016), multidecadal variability of extreme sea levels (excluding MSL and long-period tidal cycles) has often been omitted, although it can modulate coastal flood risk in addition MSL changes alone (Marcos et al., 2015; Wahl & Chambers, 2015). Recently, Rashid et al. (2019) (referred to as R19 hereafter) investigated the temporal and spatial variability of MSL, extreme sea levels, and low-frequency tides (i.e., 4.4-year perigean and 18.6-year nodal cycles) for the contiguous U.S. coastline.

10.1029/2020JC016295

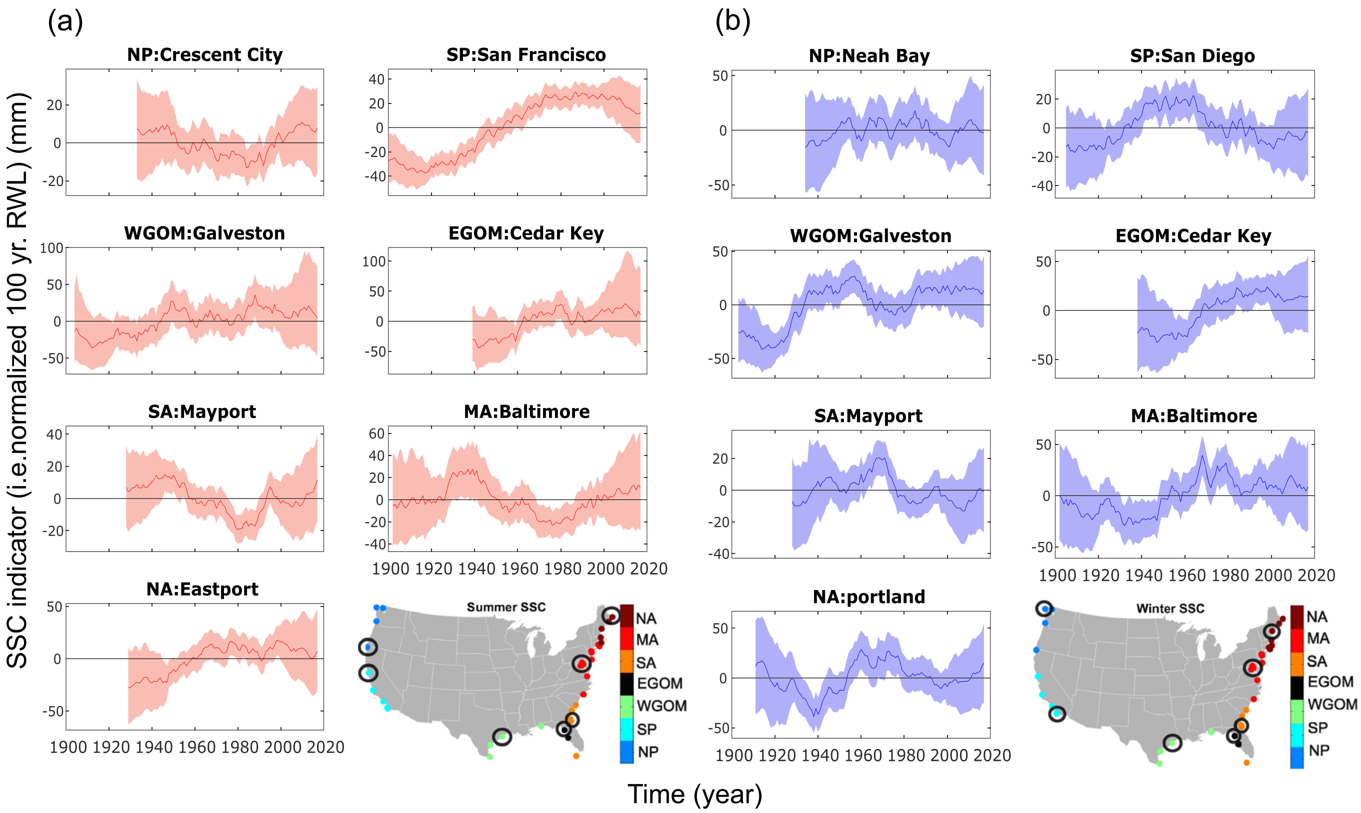

Figure 1. SSC indicators of different coherent regions representing the 100-year RWL variability (in mm) around the long-term mean and corresponding uncertainty bands (at one-sigma level) for summer (a) and winter (b) seasons. Maps represent the spatial domain of coherent regions. (NP: U.S. northern Pacific coast, SP: U.S. southern Pacific coast, WGOM: western Gulf of Mexico, EGOM: eastern Gulf of Mexico, SA: South Atlantic, MA: Mid-Atlantic, NA: North Atlantic). Black circles indicate the geographical locations of representative tide gauges.

R19 developed separate indicators for MSL and storm surge climatology (SSC) and aggregated them with perigean and nodal tidal fluctuations (i.e., multiyear tides) to derive an extreme sea level indicator. In order to develop SSC indicators, first, MSL (long-term trends and variability) and influences of multiyear tides were removed, and hourly water level residuals from 35 tide gauges were used to develop time series of seasonal maximum water levels. The two seasons, or half-years, considered for the analysis correspond to the tropical and extratropical storm periods (tropical/summer from May to October and extratropical/winter from November to April). Seven regions of coherent SSC variability along the contiguous U.S. coastline were identified using *k*-means clustering. For each tide gauge, changes in the 100-year return water level (RWL) were estimated with a quasi-nonstationary extreme values analysis. Among the tide gauges within each coherent region, a representative tide gauge was identified as the one that best represents the regional variability of 100-year RWL (i.e., 100-year RWL time series averaged over all tide gauges within the region) and has the maximum record length. Hence, the SSC indicator represents the coherent 100-year RWL multidecadal variability for seven regions and two seasons (normalized versions of the indicator with the mean of the entire period subtracted are shown in Figure 1).

Decadal to multidecadal variations in the SSC indicators are evident and vary significantly across regions and seasons (Figure 1). The ranges of temporal fluctuations (i.e., the difference between maximum and minimum values) of SSC indicators (which are unrelated to MSL) are in the order of 1 to several centimeters. This highlights the potential implications of SSC variability in addition to long-term MSL changes, which is often the only oceanographic driver considered in coastal flood risk analysis. Understanding and prediction of these variations would lead to better short- to medium-term risk assessments and robust adaptation planning.

Teleconnections of extreme sea levels and large-scale climate variability were highlighted in various studies, where climate indices related to the El Niño Southern Oscillation (ENSO) phenomena such as Southern Oscillation Index (SOI), North Pacific Index (NPI), Pacific Decadal Oscillation (PDO), Multivariate ENSO Index, Niño 2.1, and Niño 3.1 were often linked to storm surge variability along the U.S. coasts (Bromirski et al., 2003, 2017; Cayan et al., 2008; Komar et al., 2011; Serafin & Ruggiero, 2014; Wahl & Chambers, 2016). Additionally, the North Atlantic Oscillation (NAO) and Atlantic Multidecadal Oscillation (AMO) were linked to SSC along the Gulf of Mexico and South Atlantic coasts, particularly during tropical cyclone season (May–October) (Kennedy et al., 2007; Park, Obeysekera, & Barnes, 2010; Park, Obeysekera, Irizarry-Ortiz, et al., 2010), as well as the Mid-Atlantic and North Atlantic coasts (Sweet & Zervas, 2011; Talke et al., 2014). These studies mainly focused on the interannual variability of extreme sea levels or SSC. Large-scale climatic mechanisms that influence the decadal to multidecadal variability of extreme sea levels may be different from the traditional climate indices (Dangendorf, Müller-Navarra, et al., 2014; Marcos et al., 2015; Thompson et al., 2013; Wahl & Chambers, 2016). For example, tailored climate indices formulated from sea level pressure (SLP) and sea surface temperature (SST) explain the multidecadal variability of extreme sea levels better than the traditional climate indices (Wahl & Chambers, 2016). While these studies identified potential predictors (traditional and tailored climate indices) and reconstructed observed variations, they did not perform a rigorous validation in terms of the predictability of extreme sea level variability. A natural next step would also be to assess the merit of using simulated climate information (e.g., large-scale SLP and SST patterns) from initialized decadal climate models to predict the extreme sea level variability (i.e., SSC indicators), which has not been attempted yet.

In a natural system, one often needs to predict a response that exhibits temporal variability differently to its potential predictor variables. Conventional regression modeling approaches (whether linear or nonlinear) poorly model responses characterized in the frequency spectrum differently to its potential predictor variables. An alternative is to transform the variance of time series into different time scales (or frequency bands) and use regression models to build the relationships between responses and predictors in the frequency domain. Wavelet Transform (WT) is a powerful mathematical tool often used for such variance transformation by decomposing the original time series into low frequency and high-frequency subseries. Analysis and modeling in the frequency domain to understand the response-predictor relationships and to predict variability in the target response have been proven to be a useful tool for various applications (He & Guan, 2013; Jiang et al., 2020; Rashid et al., 2016, 2018; Rashid & Beecham, 2019).

We examine three modeling experiments using different predictor data sets to assess the predictability of SSC indicators along the contiguous U.S. coastline over the period from 1900 to 2017. The three modeling experiments use different predictor information: (1) traditional climate indices, (2) tailored indices from reanalysis SLP and SST, and (3) tailored indices derived from SLP and SST of initialized decadal climate model simulations. The first experiment allows evaluating the wavelet-based modeling framework proposed in this study, the second one assesses the merit of tailored indices, and the third one explores, for the first time, the predictability of decadal SSC variability using tailored predictors of SLP and SST from initialized decadal climate model simulations.

2. Data

Hourly sea level data from tide gauges along the contiguous U.S. coastline were used to derive SSC indicators. Data came from three different sources: University of Hawaii Sea Level Center (UHSLC; http://uhslc.soest.hawaii.edu/data/download/rq), Global Extreme Sea Level Analysis (GESLA; http://gesla.org/), and National Oceanic and Atmospheric Administration (NOAA; http://tidesandcurrents.noaa.gov/). MSL and long-period tidal fluctuations (4.4-year perigean and 18.6-year nodal cycles) were removed, and residuals were used to develop seasonal (summer and winter half of the year, i.e., May to October and November to April) maximum water level time series. SSC indicators are the 100-year nonstationary RWLs derived from the seasonal maximum water levels. Further details of preprocessing of the water level data and derivation of SSC indicators are outlined in R19. Here, for three different modeling experiments, large-scale climate indices, reanalysis, and initialized decadal climate model experiment data were obtained from different sources. Eight climate indices, previously identified to potentially influence SSC variability along the U.S. coast, are considered in this study: AMO, Atlantic Oscillation (AO), NAO, Niño 1.2 (N12), Niño 3 (N3), NPI, PDO, and SOI. These indices represent SLP and SST anomalies in different spatial domains.

To develop tailored indices, we use SLP and SST from reanalysis and decadal climate model outputs. For reanalysis monthly SST data, we use NOAA's Extended Reconstructed SST V4 from 1851 to 2017 with a spatial resolution of 2° × 2°. Monthly SLP data were obtained from NOAA-CIRES 20th century reanalysis (V2c) with temporal coverage from 1851 to 2014 and spatial resolution of 2° × 2°.

Decadal climate model retrospective forecasts of monthly SLP and SST were downloaded from the Climate Model Intercomparison Project Phase 5 (CMIP5) archive. Decadal climate experiments are initialized with observational data similar to seasonal forecasting systems but also account for changes in external forcing, such as aerosols, volcanic forcing, greenhouse gases, and solar activity. Recent studies reported that the decadal models show skills in forecasting climate variables (e.g., SLP and SST) from a few months to several years (Choudhury et al., 2015; Matei et al., 2012; Saurral et al., 2020; Smith et al., 2019). Decadal forecasts from the CMIP5 archive are used in different studies (e.g., Choudhury et al., 2019; Salvi, Villarini, & Vecchi, 2017; Salvi, Villarini, Vecchi, & Ghosh, 2017). Here, we focus on NOAA's Geophysical Fluid Dynamics Laboratory (GFDL) decadal climate experiment (GFDL-CM21) for testing purposes, but note that outputs from other models are also available. GFDL-CM21 is a full-field initialization decadal climate model that initialized every year from 1961 onwards and provides 10 years ($12 \times 10 = 120$ months) forecast at each initialization. We consider the initialization period from 1961 to 2005, thus dealing with 45 overlapping decadal forecasts (i.e., 1961–1970, 1962–1971, ..., 2005–2014) of SLP and SST.

3. Methods

We develop models using SSC indicators as predictands and traditional large-scale climate indices, as well as tailored indices (based on SLP and SST) obtained from reanalysis and decadal climate model experiments (i.e., GFDL-CM21) as predictors. Models are developed separately for each region, season, and source of the predictor variables. First, we employ wavelet decomposition to derive filtered subseries corresponding to different frequency bands and identify potential predictors using correlation analysis but with a modified significance testing (see section 3.2 for more details). Then, we formulate models in the frequency domain fitting separate regression models for each frequency band.

3.1. Wavelet Decomposition

We start with monthly time series of the predictor variables (i.e., climate indices, SLP, and SST) and develop seasonal series by averaging monthly values corresponding to the seasons (tropical/summer: May to October; extratropical/winter: November to April). For the gridded SLP and SST data, the analysis was performed for each grid location. We then decompose the seasonal annual series of SSC indicators and predictor variables into a number of smooth subseries corresponding to different frequency bands using discrete wavelet transform (DWT). Daubechies wavelet function (Daubechies, 1988) was used to decompose the data into five predefined frequencies, varying from multiyear to decadal. The Daubechies wavelet is an orthogonal wavelet that decomposes time series into a set of mutually orthogonal details, where each detail represents the variability of the time series at a particular frequency. Short-period frequency (subannual to annual) details (D1 and D2 in Figure 2) capture rapidly varying events in the time series, whereas low-frequency (multiyear to decadal) details (D3 to D5 in Figure 2) contain information on slowly varying events. The approximation (A5) represents the remaining low-frequency residuals in the time series. Wavelet decomposition of the time series results into vectors of coefficients at each frequency band. Using an inverse DWT, six (five details and one approximation) filtered time series corresponding to specific frequency bands are reconstructed from the respective vector of wavelet coefficients. Thus, filtered subseries of SSC indicators and predictor variables were derived to model each subseries separately using corresponding significant predictors identified through correlation analysis.

3.2. Correlation Analysis

Pearson correlation coefficients between filtered subseries of SSC indicators and climate predictors are used to identify the significant predictors. Due to strong autocorrelation in the filtered subseries, we adopt an alternative approach for significance testing. The observed correlation is tested against the correlation obtained from lag-1 red noise, employing a Monte Carlo simulation following these steps:

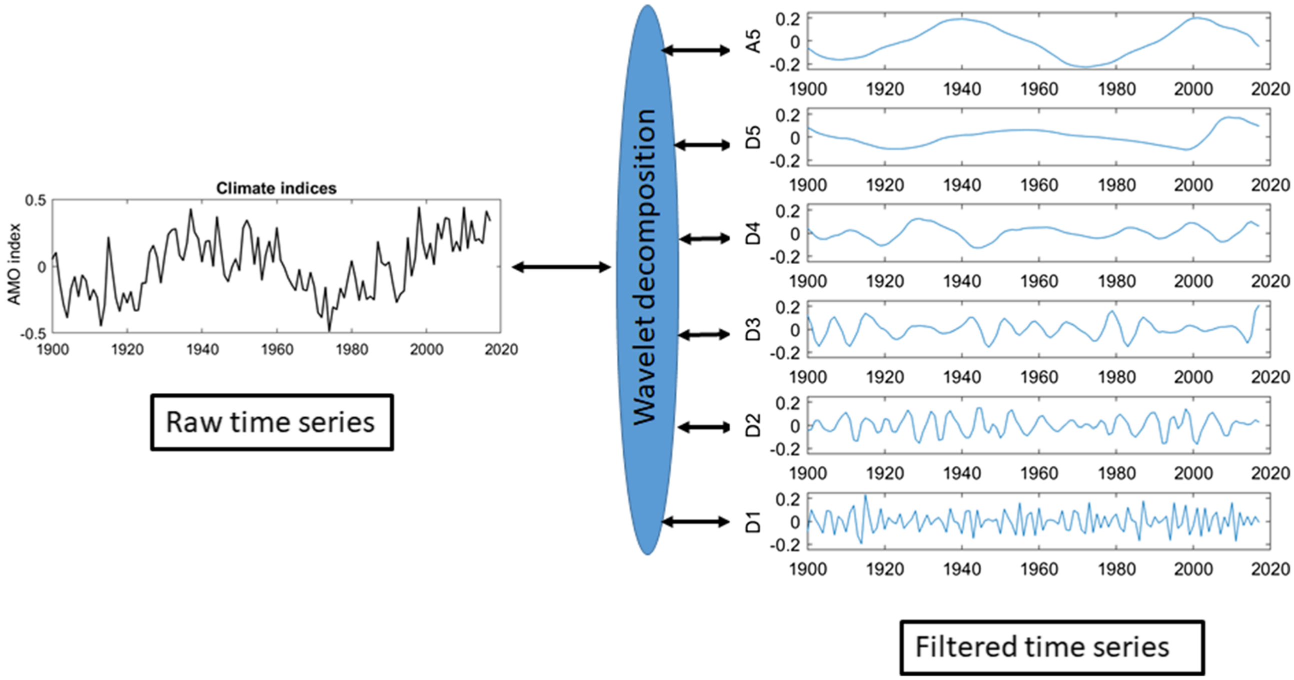

Figure 2. Decomposition of time series by discrete wavelet transform (DWT) using Daubechies wavelet.

1. Estimate correlation between the filtered time series of SSC indicator and climate index.
2. Estimate lag-1 autocorrelation of the filtered time series of SSC indicator and climate index and generate 1,000 random red noise time series with estimated lag-1 autocorrelation.
3. Estimate correlation with each of the simulated red noise time series.
4. Define the significance band as the 2.5th and 97.5th percentiles of the 1,000 correlation coefficients.
5. Compare the correlation coefficient estimated in Step 1 with the significance band derived in Step 4; if the correlation coefficient falls outside the significance band, it is significant at a 5% significance level.

In addition to this procedure, we also employed a *t* test that accounts for the reduced number of degrees of freedom due to the smoothing and tested deriving the red noise estimate from the raw data and then applying the smoothing. Both methods are less restrictive than the one outlined above (i.e., correlation needs to be stronger to be deemed significant with the method we employed).

3.3. Identifying Significant Predictors

As outlined above, we derive filtered subseries of SSC indicators and different predictor variables. For each SSC indicator subseries, we estimate correlation coefficients with the corresponding subseries of the predictors and retain the subseries that provides the strongest relationship (at the 5% significance level). This procedure is straightforward when using traditional climate indices.

To derive the tailored indices, which are based on gridded SLP and SST data, we estimate correlation coefficients between the SSC subseries (predictand) and corresponding subseries of SLP and SST (predictors) at each grid location to identify regions of significant correlation (termed as the center of action) using the wavelet decomposition method outlined in the previous section. The tailored indices are then derived by averaging the SLP or SST subseries across grid locations within the center of action. The following steps are involved in deriving the tailored indices:

1. For a frequency band, estimate correlation coefficients of SSC indicator and climate variable (SLP or SST) at each grid location resulting in a 2-D correlation coefficient matrix (Figure 3a).
2. Apply *k*-means to the correlation matrix from (1) to form clusters of grid locations based on proximity and similarity in correlation coefficients. Identify clusters where correlation coefficients are statistically significant (Figure 3b). Red circles in Figure 3b represent the clusters corresponding to negative

10.1029/2020JC016295

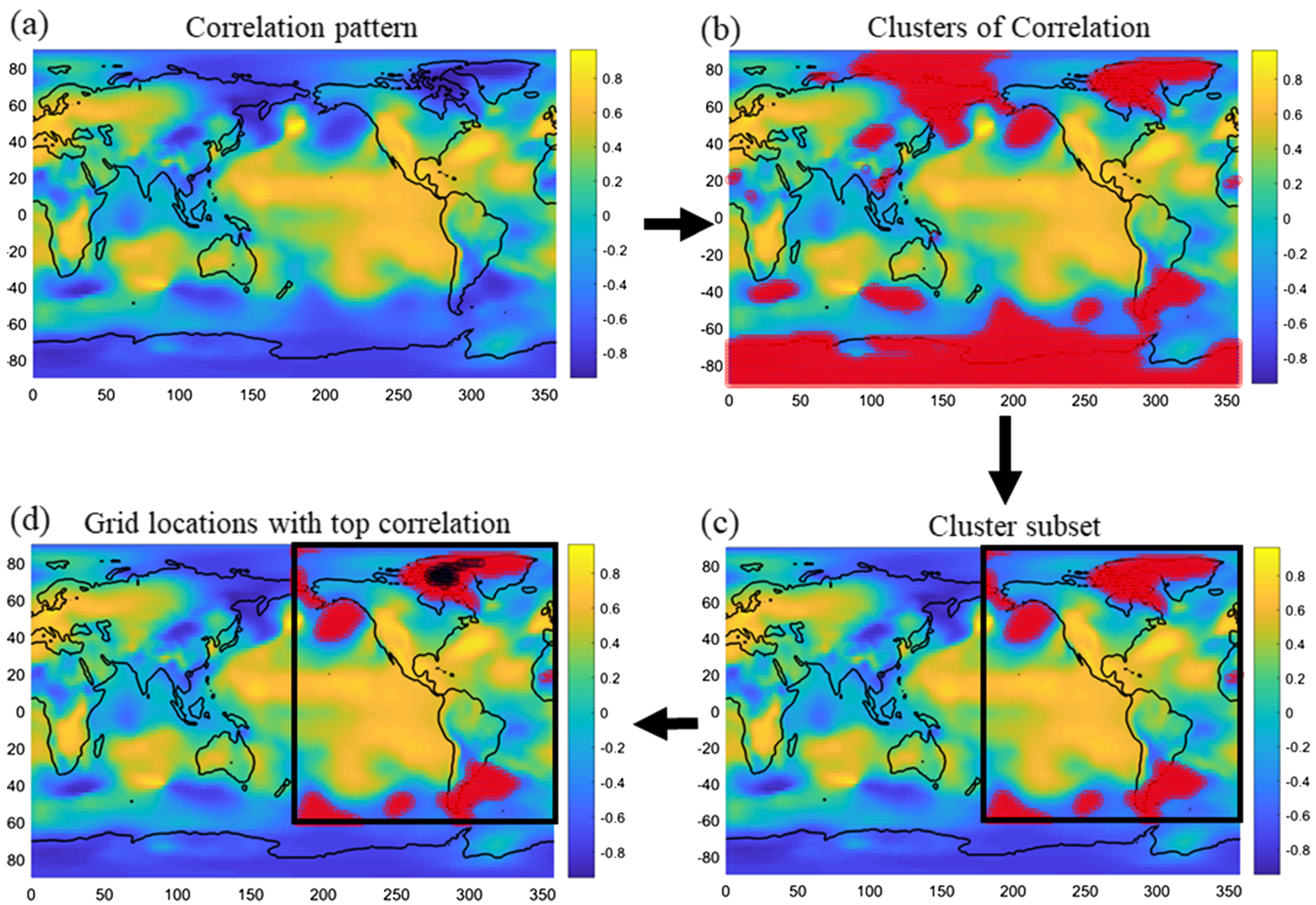

Figure 3. Algorithm for the development of tailored indices using gridded SLP and SST data from reanalysis or decadal climate model for a typical frequency band. Color map represents correlation coefficients of SLP and SSC indicators (a). Clusters of significant correlation are shown as red dots (b). Subsets of clusters within the regions enclosed by the black rectangle we focus on for predictor selection (c). Grid locations (shown as black dots) with top 5% correlation coefficients within the cluster with the highest correlation (d). *x* and *y* axes represent latitude and longitude, respectively.

correlation coefficients; clusters corresponding to positive correlation are also obtained but not shown for clarity.

3. Identify clusters falling within the black rectangle in Figure 3c. This region is considered because storms causing extreme surges along the U.S. coastlines are generally modulated by the atmospheric and oceanic conditions in this region (Bromirski et al., 2017; Wahl & Chambers, 2016)
4. Estimate the average correlation of each cluster and select the cluster that has the maximum average correlation for further analysis. From the selected cluster, identify the grid locations within 5% of the correlation maxima (black circles in Figure 3d).
5. Repeat Steps 1 to 4 for both SLP and SST and consider the one with the higher correlation as the significant predictor.
6. Develop tailored indices by averaging SLP or SST subseries (derived in Step 5) of the grid locations identified in Step 4.
7. Develop tailored indices for each frequency band following Steps 1–6.

3.4. Developing Prediction Models With Traditional and Tailored Climate Indices

As mentioned earlier, we employ wavelet decomposition to derive filtered subseries of SSC indicators and predictor variables (i.e., climate indices, SLP, or SST) corresponding to predefined frequency bands (D1 to D5 and A5). With the predictors (from traditional or tailored climate indices) identified with the approach described in sections 3.2 and 3.3, we develop linear regression models for the different frequency bands

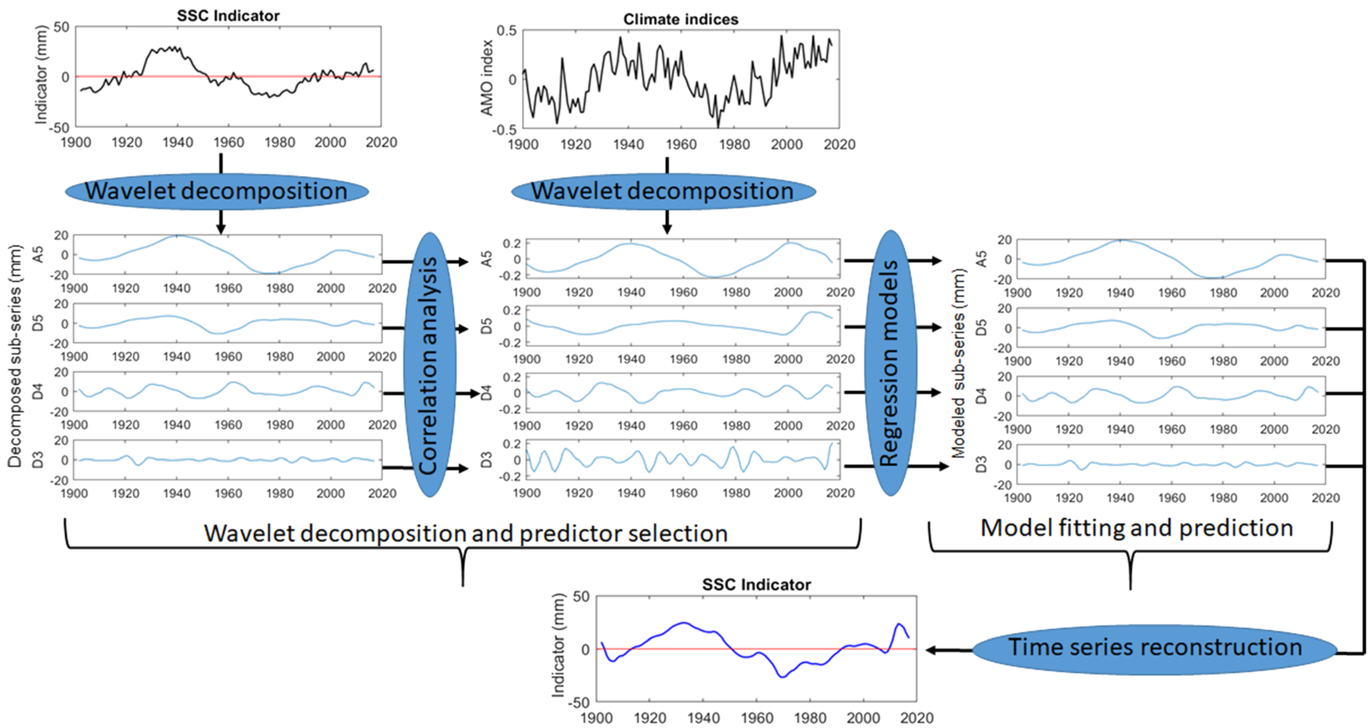

Figure 4. Flow diagram outlining the formulation of the SSC indicator prediction models, starting with the SSC indicator (predictand) and climate indices (predictor) (top), decomposed versions of them (left), prediction results at different frequency bands (right), and reconstructed SSC indicator based on the predictions at different frequency bands (bottom).

separately and predict associated subseries of SSC indicators. To mitigate possible violations of regression model assumptions due to autocorrelated error terms, we employed the Newey-West method (Newey & West, 1986), where model parameters (e.g., standard errors and covariance matrix) are obtained from the ordinary least square (OLS) method but adjusted to account for autocorrelation and heteroscedasticity in the error terms of the models. We focus on frequency bands D3, D4, D5, and A5, as these contain the relevant information on multiyear to multidecadal variability. Finally, SSC indicators are reconstructed by aggregating the predicted subseries. As we used DWT with Daubechies wavelet (which is an orthogonal wavelet) to develop filtered subseries, it allows perfect reconstruction of the original time series by adding filtered subseries. Steps followed in the modeling framework are presented in Figure 4. The key innovation of the modeling approach adopted in this study is to identify the most important frequency bands of predictor variables using wavelets to improve the strength of correlations with SSC indicators and developing models in the frequency domain. This allows a robust prediction of SSC indicators compared to a model setup with unfiltered predictands and predictors. For validation of the modeling approach, we consider the first 60% of the data to fit the model and the remaining 40% for validation.

3.5. Testing Predictability With Decadal Climate Model Outputs

We develop models for decadal prediction of SSC indicators using CMIP5 decadal retrospective forecasts of SLP and SST obtained from initialized decadal climate model experiments. Drift correction is recommended for CMIP5 decadal forecasts (ICPO, 2011). Here, we employ a trend-based drift correction method proposed by Kharin et al. (2012) that includes an additional time-dependent trend adjustment in addition to the standard drift correction where the lead time-dependent mean drift is estimated. Trend-based drift correction provides the lowest errors, for example, in estimating SST based climate indices, compared to other methods (Choudhury et al., 2017). Before drift correction, decadal climate model outputs were regridded to reanalysis grid resolution. As mentioned in section 2, we use the output from GFDL-CM21 for this study, which is initialized every year from 1961 onwards and forecasts SLP and SST for the next 120 months (referred to as lead time). A total count of 45 model initialization years, including 45 overlapping decades (1961–1970,

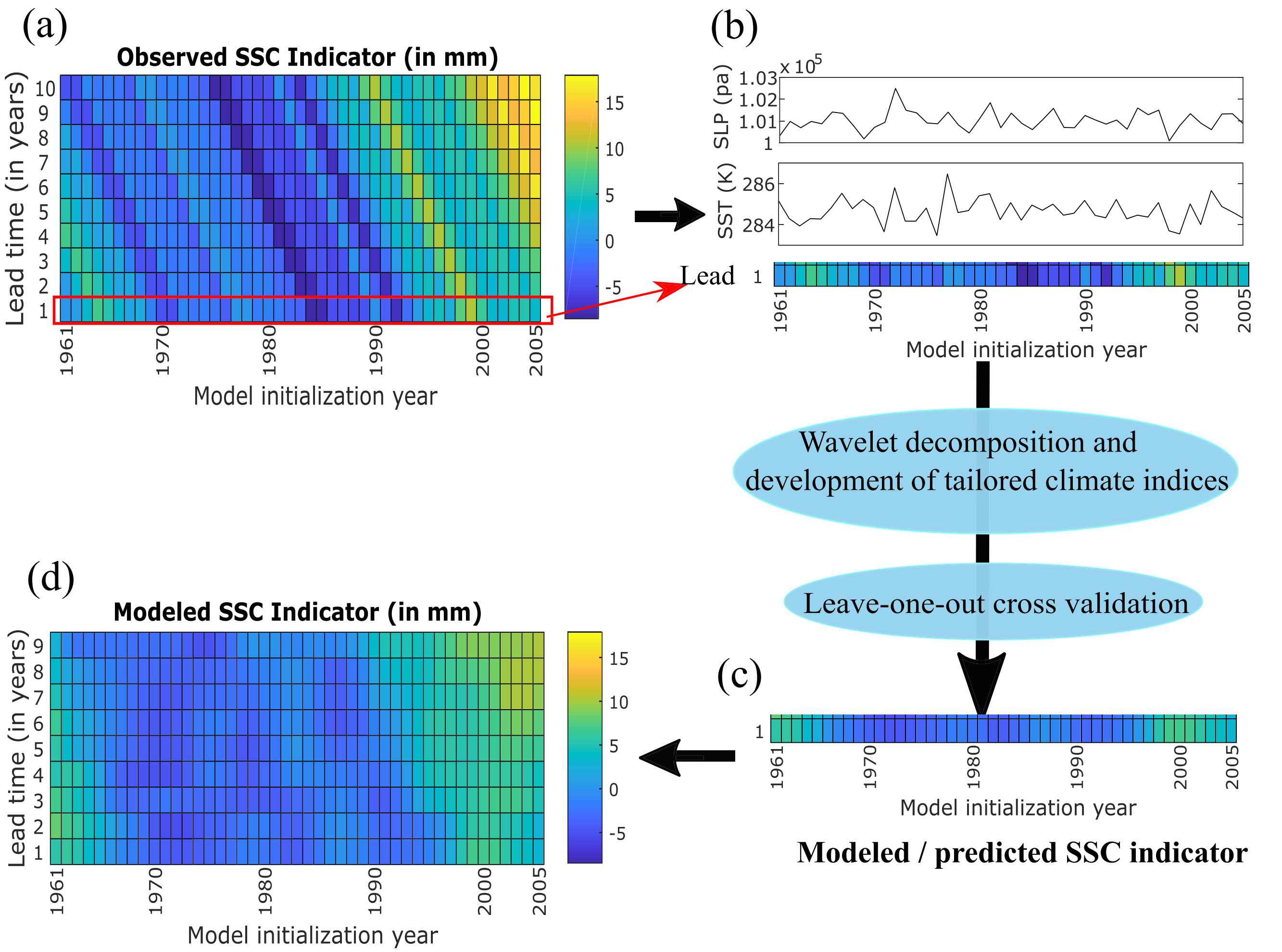

Figure 5. Flow diagram outlining the prediction of SSC indicators using SLP and SST of decadal climate model outputs. Color plots of observed SSC indicator time series are arranged to match with the GFDL-CM21 data structure, and color bars represent the values of the SSC indicator (in mm) (a). Observed SSC indicator at lead time 1 (color plot) and corresponding SLP and SST time series of a typical grid location (b). Modeled SSC indicator for lead time 1 (c). Modeled SSC indicators for lead times 1 to 9 (d). In each color plot (a and b), the *x* axis represents model initialization years (1961–2005), and the *y* axis represents lead times (in years).

1962–1971, ..., 2005–2014), is used, leading to a 120 × 45 data matrix at each grid location for each climate variable. We convert monthly forecasts of SST and SLP into seasonal time series by averaging monthly values corresponding to each season (summer or winter), reducing the data matrix to 10 (lead time in years) × 45 (number of model initializations). However, for the winter season (which is the average of values from November to December of the current year and January to April of the next year), we cannot estimate a seasonal average for lead time 10 because no forecast is available after December. Therefore, the data matrix reduces to 9 (lead time in years) × 45 (number of model initializations) for both SLP and SST at each grid location and for each season.

For model development, we first rearrange the observed SSC indicator time series to match with the data structure of GFDL-CM21, as shown in Figure 5 (the *x* axis represents model initialization years and the *y* axis represents lead times 1 to 10). As an example, model initialization year 1961 includes 10 SSC indicator values from 1961 to 1970, corresponding to lead times 1 to 10 (in years), and model initialization year 1962 include 10 SSC indicator values from 1962 to 1971, and so on (Figure 5). This will form an SSC indicator data matrix of 10 (lead time in years) × 45 (number of model initializations). As discussed earlier, we limit our analysis up to lead time 9, as sufficient forecast data are not available to calculate winter average SLP and SST for lead time 10. We develop prediction models for each lead time separately employing a leave-one-out cross-validation approach that involves the following steps:

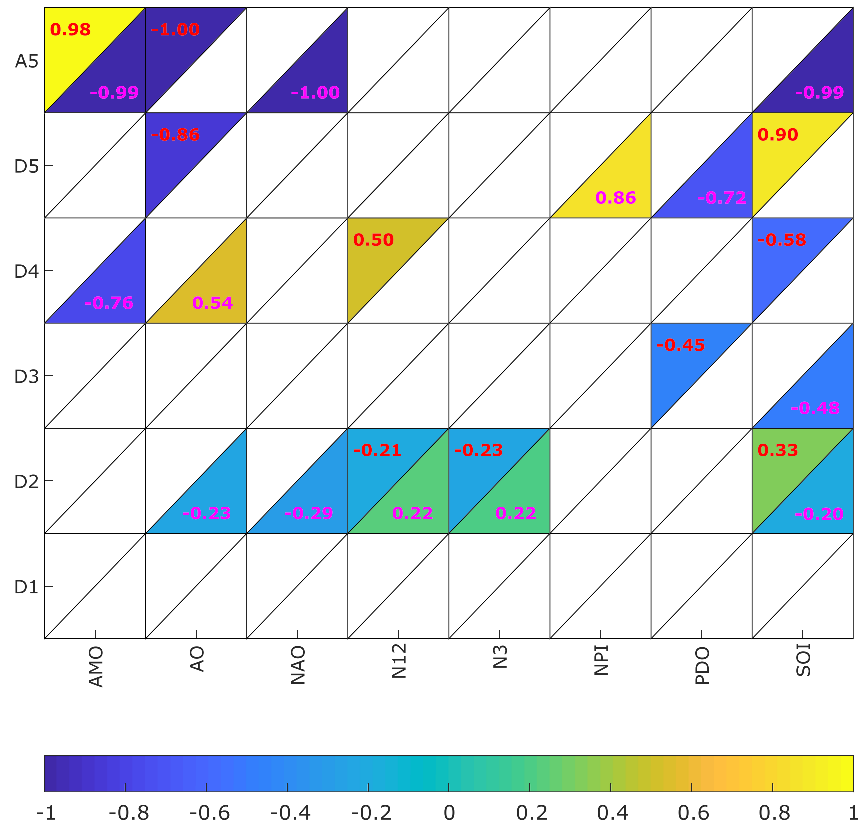

Figure 6. Correlation of the SSC indicators of the U.S. northern Pacific coast (as an example) with climate indices at selected frequency bands. D1 to D5 represent details, and A5 represents the approximation component of the time series obtained from DWT decomposition. In each rectangle, the top triangle represents the summer season, and the bottom triangle represents the winter season. Numerical values in the triangles represent magnitudes of correlation coefficients, and white triangles indicate insignificant correlation.

1. Select an SSC indicator corresponding to lead time 1 from the rearranged SSC indicator matrix (10×45); this results in a time series consisting of 1×45 SSC indicator values rolling from 1961 to 2005. Employ wavelet to decompose the SSC indicator time series into subseries corresponding to selected frequency bands (see section 3.1).
2. For each grid location, subset SLP and SST corresponding to lead time 1 results into time series of 1×45 values from 1961 to 2005. Decompose the SLP and SST time series into subseries corresponding to selected frequency bands.

   a. For each subseries of SSC indicator (obtained in Step 1), estimate correlation with corresponding subseries of SLP and SST at each grid location (obtained in Step 2) and develop tailored indices (by identifying significant predictors) following the procedure outlined in section 3.3.
   b. As a result of (a), subseries of the SSC indicator and corresponding tailored indices have 1×45 values corresponding to 45 initialization years. Leave one value corresponding to a specific initialization year out for validation and use remaining values for training. Train a regression model and predict the SSC indicator for the specific initialization year that was left out. Repeat model training and prediction for each initialization year, resulting in predicted subseries of the SSC indicator.
   c. Repeat Steps (a) and (b) for all subseries and reconstruct the SSC indicator through aggregating the predicted subseries.

3. Repeat Steps (1) and (2) to predict the SSC indicator time series corresponding to other lead times.

10.1029/2020JC016295

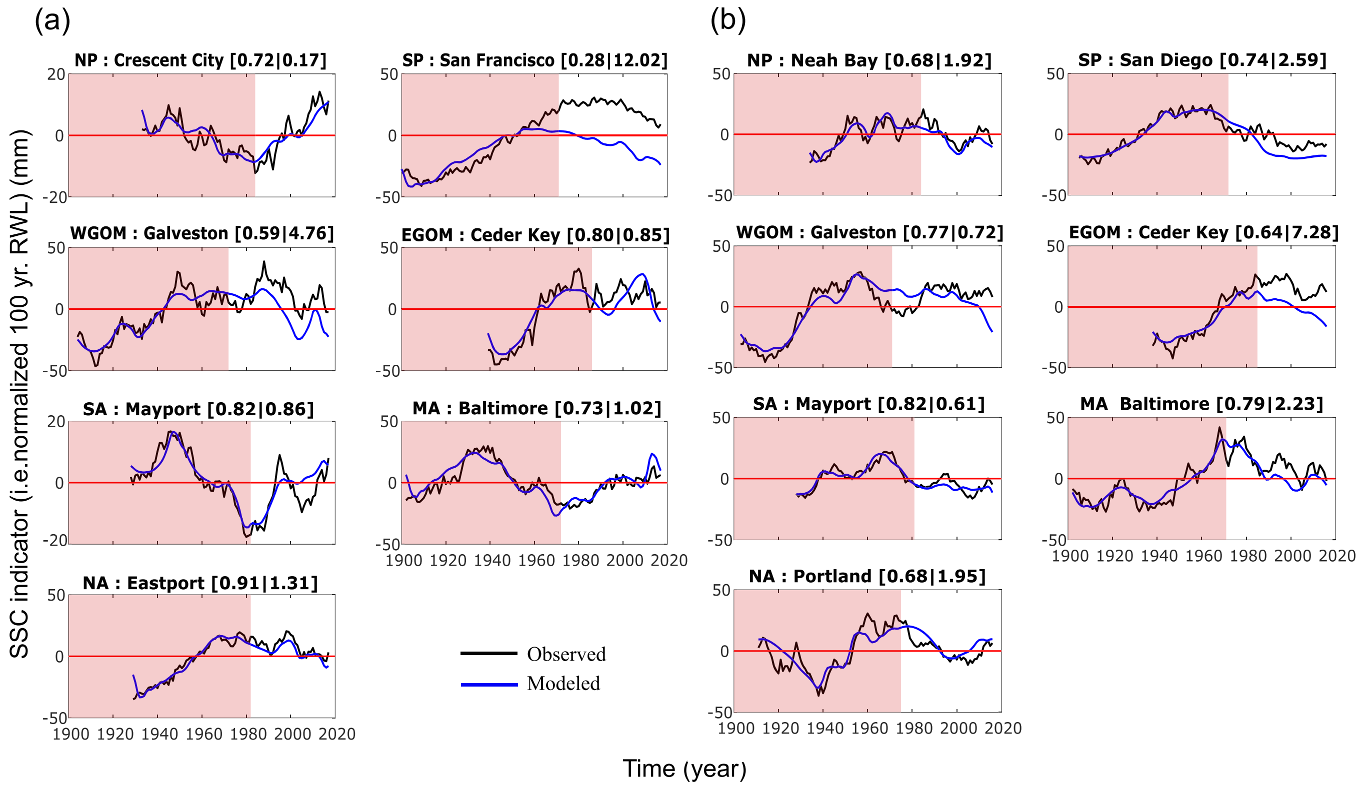

Figure 7. Observed (black lines) and predicted (blue lines) SSC indicators (considering filtered traditional climate indices as predictor variables) for different coherent regions for the summer (a) and winter (b) seasons. Red shaded areas represent the calibration periods, and white areas represent the validation periods. Numeric values in the title of each subplot represent model efficiency statistics [Nash-Sutcliffe efficiency|root mean square error]. Model efficiency statistics are estimated considering the entire periods covered by the SSC indicators.

4. Results

We develop models in the frequency domain to robustly predict SSC indicators from R19 through enhancing relationships with predictor variables (i.e., climate indices, SLP, or SST). Correlation coefficients of unfiltered raw SSC indicators and predictor variables (for traditional climate indices) are often weak and insignificant because the temporal variance of SSC indicators is significantly different from the climate indices. This is also true for correlations between SSC indicators and gridded SLP and SST data. In contrast, correlations are stronger and often significant when filtered subseries of SSC indicators and climate indices are considered. Figure 6 shows correlation coefficients of the SSC indicators for summer (upper triangle in each square) and winter (lower triangle in each square) for the U.S. northern Pacific coastline, as an example, with selected climate indices at different frequency bands. The strength of correlation varies across climate indices, seasons, and frequency bands. For example, in the case of A5, AO is the most dominating index in summer, whereas for D4, SOI shows the strongest correlation for the same season. Note that at rapidly varying short-period frequency bands (i.e., D1 and D2), correlation coefficients are often weak and insignificant. The results reveal that wavelet transform is useful to identify the most prominent frequency bands as well as to improve the strength of correlations, which eventually enhances the prediction of SSC indicators.

4.1. Prediction of SSC Indicators Using Traditional Climate Indices

As discussed in section 3, we fitted regression models separately for each frequency band (D3 to D5, and A5) using corresponding filtered subseries of SSC indicators (predictands) and climate indices (predictors). For each regression model, the climate index that shows the highest correlation with the SSC indicator is considered as the significant predictor. Significant predictors used in the regression models vary with coastal regions, seasons, and frequency bands. Figure 7 shows observed and predicted SSC indicators for each region and season after aggregating the predicted subseries for different frequency bands. Each SSC indicator is presented as a normalized time series (i.e., long-term mean is subtracted). The results indicate that the models reproduce overall trends and variability of the SSC indicators well for all regions and seasons, with the exception of the U.S. southern Pacific (SP) coast in the summer season, where San Francisco was selected as the reference tide gauge in R19. For this particular case, the model underestimates in the validation period, although it performs well in the calibration period. This suggests that the relationships of the SSC indicator and the best possible predictor variables from the climate indices are not consistent over the entire analysis period. However, the model performance improves when tailored indices are used as predictors (see section 4.2).

4.2. Prediction of SSC Indicators Using Tailored Indices

We developed tailored indices through averaging reanalysis SLP or SST of grid locations where the strongest correlations with SSC indicators were observed (see section 3). In most cases, the center of actions identified in developing tailored indices roughly resemble the spatial domain of traditional climate indices used in this study but represent a refinement for the specific task. For clarification, clusters with the highest correlation between SLP/SST and SSC indicators (i.e., center of actions) for selected regions at the A5 frequency band are shown in Figure S1 in the supporting information. Results indicate that the spatial distribution of identified clusters (highlighted by black circles) with strongest correlations are often comparable with well-known large-scale atmospheric patterns where the physical mechanisms that connect them with extreme sea level variability are understood. For example, AO and NAO type teleconnections are observed for the NP, SA, and NA regions, whereas clusters identified for the GOM region resemble the ENSO teleconnection, and we also find interhemispheric teleconnections for the SP region. Similar relationships between low-frequency variability of extreme sea levels and large-scale atmospheric circulation patterns were also found in earlier studies (Dangendorf, Müller-Navarra, et al., 2014; Wahl & Chambers, 2016). However, traditional climate indices are often formulated by averaging SLP/SST over large spatial domains, which may dampen the inherent temporal variability important to capture the variance of SSC indicators. Thus, we develop indices tailored to SSC indicators by selecting subregions (grid locations with top 5% correlation coefficients; see section 3) from the larger spatial domains where significant correlation exists. This enables us to derive robust and temporally consistent tailored indices leading to the efficient prediction of SSC indicators.

Once tailored indices are formulated, we fit regression models and predict SSC indicators in the same way we do with traditional climate indices. The models capture most of the variability of SSC indicators in different regions for the summer and winter seasons (Figure 8). Model efficiency statistics (Nash-Sutcliffe efficiency and root mean square error) indicate that the models perform better than the ones using traditional climate indices (with very few exceptions, where Nash-Sutcliffe efficiency values drop minimal compared to the ones derived with traditional indices, e.g., WGOB and SA regions for the winter season). This includes significant improvement for the SP region in the summer season (Figure 8), where the model with traditional climate indices performed poorly (Figure 7). Arctic Oscillation (an atmospheric circulation pattern over the mid-to-high latitude of the northern hemisphere) was found as the significant predictor from traditional climate indices, whereas our tailored index represents an interhemispheric teleconnection with SLP over the southeastern region of New Zealand. While such interhemispheric teleconnections were observed in earlier studies for precipitation variability in the southwestern United States (Mamalakis et al., 2018), a more detailed analysis is warranted to explore the underlying dynamics (but this is beyond the scope of the analysis presented here).

Previous studies use simpler modeling frameworks (simply linking low-pass filtered SSC indicators to low-pass filtered climate indices) than the one proposed here (based on wavelet transform and allowing linking information from different climate indices at different frequency bands to the respective SSC frequency bands). A simple visual comparison of the results presented here with the ones from Wahl and Chambers (2016) (they used 37-year running mean) reveals that our approach improves the prediction of SSC indicators. To demonstrate this quantitatively, we also compared our results with those obtained from a model setup that only uses the long-term low-frequency residual component (i.e., A5; explaining the maximum variance of the SSC indicators) obtained from the wavelet decomposition. Note that this is essentially a low-pass filtered version of the indices (at approximately the 32-year frequency band given the way the wavelet transform was implemented). Comparing Nash-Sutcliffe efficiency statistics indicates that the

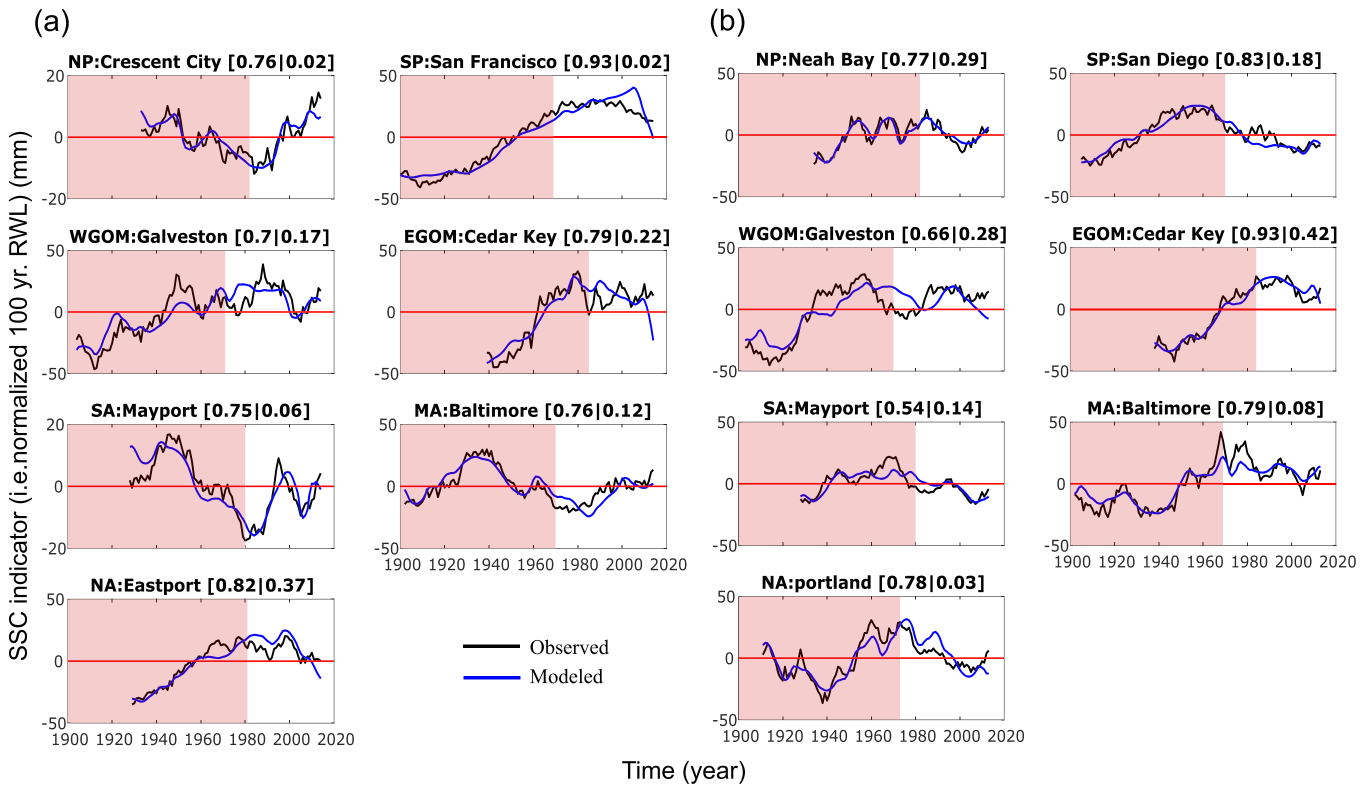

Figure 8. Same as Figure 7, but SSC indicators were predicted with tailored indices derived from reanalysis SLP and SST.

wavelet-based approach outperforms this simplified "reference model" (see Table S1). This shows that the variability in the other frequency bands also contains significant information, and considering it in the modeling framework improves model efficiency.

4.3. Predictability of SSC Indictors With Predictors From Initialized Decadal Climate Model

We also test the predictability of SSC indicators using SLP and SST from initialized decadal climate model experiments (here GFDL-CM21). As outlined in section 3.5, for each lead time (from 1 to 9), we develop regression models and predict SSC indicators, using a leave-one-out cross validation approach. We derive tailored indices from drift corrected decadal climate model SLP and SST and use those as predictors for model development and to forecast SSC indicators. We adopt this approach as opposed to using the same predictors derived from the reanalysis to ensure homogeneous and consistent predictors (i.e., tailored indices) for the model development and forecast, as suggested in earlier studies (Rashid et al., 2015; Sachindra et al., 2014). For decadal climate models in particular, Choudhury et al. (2019) used indices derived from decadal climate model SST as predictors for model development and forecast of Australian seasonal rainfall. Figure S2 shows the centers of action from which the tailored indices are derived when using the climate model output as opposed to reanalysis data (shown in Figure S1). The centers of action from which the tailored indices are derived are in the same regions for both cases, only slightly shifted, highlighting that the same physical mechanisms and large-scale teleconnections that link reanalysis data to SSC variability are captured by the climate models, leading to high correlation in the same regions.

SSC indicators are presented in Figure 9 as a 9 (lead time) × 45 (initialization years) data matrix; each column in the subplot represents the observed or modeled values of SSC indicators for lead times 1 to 9 (from bottom to top) corresponding to a single model initialization year. Overall, the models reproduce the SSC indicator variability well, leading to similar patterns in matrices representing high or low values. This is also confirmed by high (uncentered) pattern correlation ranging from 0.63 to 0.91 for the different regions and seasons (shown in brackets next to the panel titles in Figure 9), revealing the merit of using SLP and SST from initialized decadal climate models to predict SSC variability. The prediction skill is comparatively

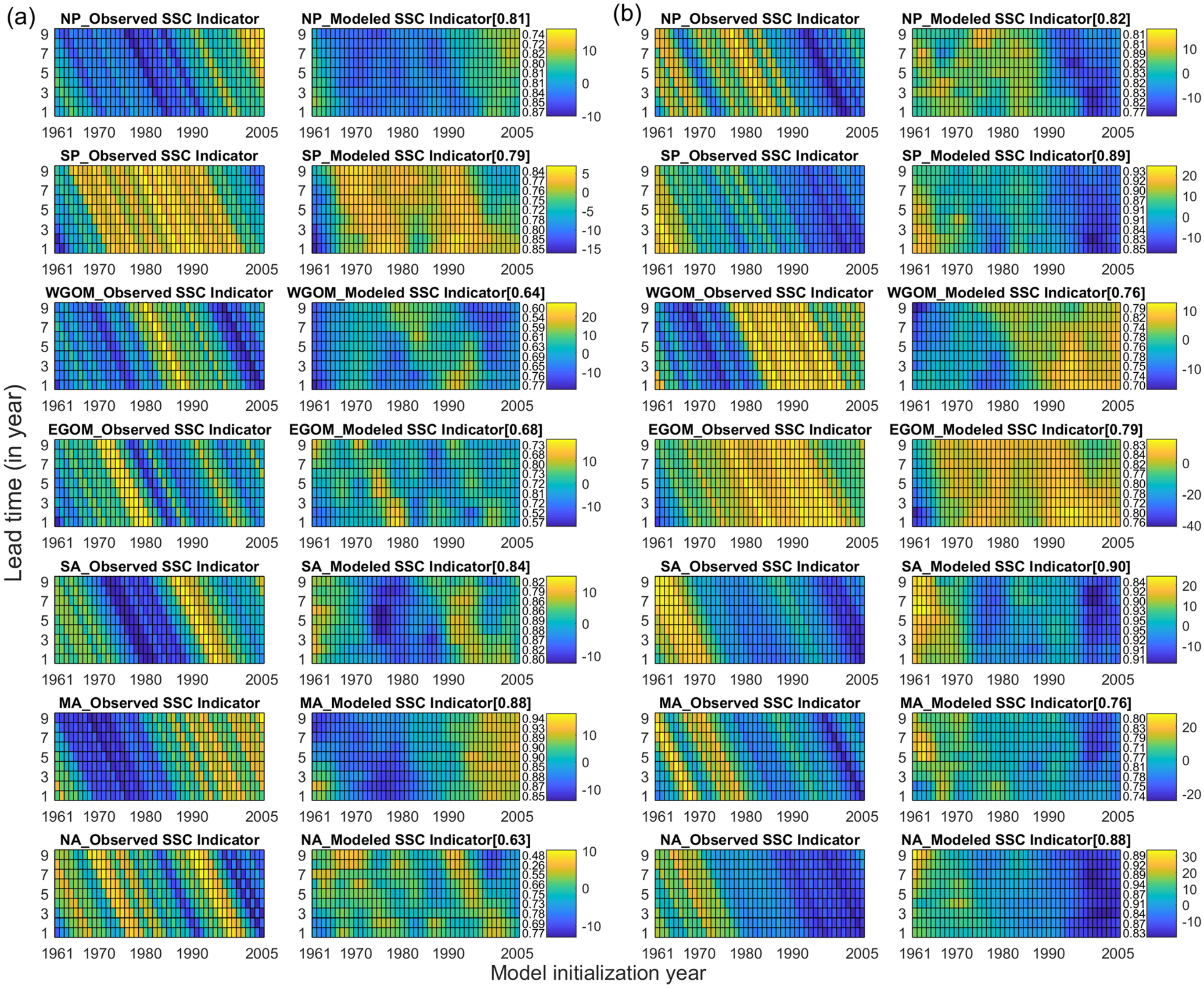

Figure 9. Comparison of observed and predicted SSC indicators over a decadal period for all regions in the summer (a) and winter (b) seasons. In each subplot, the *x* axis represents model initialization years (1961–2005), and the *y* axis represents lead times (1–9, in years). Color bars represent SSC indicator values (in mm). Numerical values in the titles of subplots (with parenthesis) represent pattern correlation coefficients. Numeric values at the end of color plots showing model results denote correlation coefficients of observed and modeled SSC indicators corresponding to each lead time (1–9 years).

lower in summer for the Gulf of Mexico (WGOB and EGOM) and North Atlantic (NA) regions. In general, the predictions are better in the winter season compared to the summer season, which is likely due to higher variability in the SSC indicators stemming from tropical cyclone activity in the summer that is not well captured in the predictors. Correlation coefficients of observed and modeled SSC indicators corresponding to lead times 1 to 9 are listed in Figure 9 for each region and season (numeric values at the end of the color plots showing the model results), highlighting that the models are skillful in reproducing the variability of SSC indicators. The skill does not decrease monotonically as the lead time increases, indicating that results for longer lead times are not always inferior than the ones for shorter lead times. This is due to the fact that we developed models separately for each lead time, and model initialization effects may also play a role (Salvi, Villarini, & Vecchi, 2017; Salvi, Villarini, Vecchi, & Ghosh, 2017).

Extending the leave-one-out cross validation, we also test model efficiency when actually forecasting SSC indicators over a decade, employing the modeling framework discussed earlier. For this, we considered 25 model initialization years, including 25 overlapping decades (1961–1970, 1962–1971, ..., 1986–1995) for

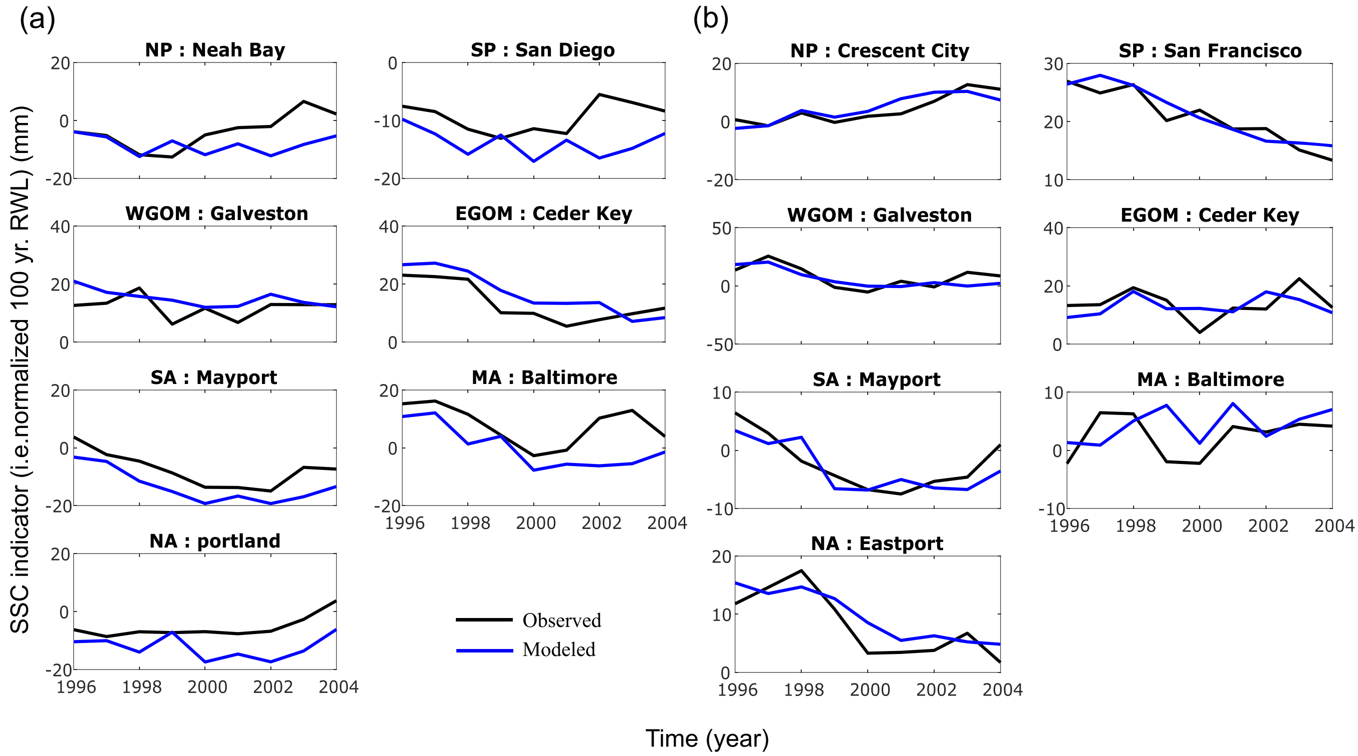

Figure 10. Observed (black lines) and forecasted (blue lines) SSC indicators (with SLP and SST from GFDL-CM21 initialized decadal simulations) for all regions in the summer (a) and winter (b) seasons.

model fitting and then drive the model with decadal simulations of SLP and SST initialized in 1996 (running from 1996–2005). As discussed earlier, we fitted separate models for each lead time. No information on SSC indicators spanning from 1996 to 2004 was used during model training (refer to Figure S3). Figure 10 represents forecasted and observed SSC indicators from 1996 to 2004. Results indicate that the models often capture the general structure and decadal trends of the SSC indicators, with some notable exceptions in the winter season when SSC forecasts deviate from observations beyond lead times of approximately 5 years. This indicates that the latest simulations of decadal climate models, initialized in the current year, can be used along with the modeling framework introduced here to assess the overall trend in low-frequency extreme sea level variations over a few years to a decade into the future. It is expected that improved climate model simulations would allow a better forecast of SSC indicators.

5. Conclusions

SSC indicators developed in R19 reflect multidecadal variability of extreme sea levels (expressed as changes in 100-year RWLs) unrelated to MSL variations. SSC variability over multidecadal time scales could have significant implications in terms of modulating coastal flood risk, where long-term MSL rise is often considered to be the only relevant oceanographic driver for changes. Therefore, developing models to predict SSC variability is crucial for coastal management. Here, we perform three different modeling experiments to assess the predictability of SSC indicators from R19; our overall results show that the developed models are capable of reproducing the general temporal behavior of the SSC indicators. Our analysis included, for the first time, an assessment of the usability of SLP and SST data from initialized decadal climate model experiments in the prediction of SSC indicators.

We introduce an innovative modeling approach where regression models are fitted in the frequency domain. This is useful for skillful predictions of responses (here SSC indicators) characterized by spectral scales significantly different from the predictors. We first decompose raw time series into filtered subseries corresponding to different frequency bands to improve the strength of correlations and then develop models separately for each frequency band. As expected, due to the mismatch in the time scales of variability, correlations among nonfiltered raw SSC indicators and climate indices are weak and insignificant in most instances. In contrast, in the frequency domain, the strength of correlation increases between the filtered subseries of predictands and predictors, and overall the models reproduce the observed SSC variability. We extended the approach to use tailored indices from gridded SST and SLP (instead of traditional climate indices) from regions with high correlation between the SSC indicators and SST or SLP after the wavelet transform. This leads to further improvements in the predictive skill of the models, especially for the summer season in the SP region, where the model with traditional climate indices underestimated the SSC variability over the validation period.

In a final step, we developed and tested models using tailored indices from SLP and SST derived from initialized decadal climate model simulations. This represents the next important step toward being able to forecast SSC variability at decadal time scales. We used SLP and SST data from one climate model (the ensemble mean) for testing purposes; this can be extended in the future to consider the full ensemble and/or a range of different climate models participating in the initialized decadal experiments. The models are capable of reproducing the general temporal behavior of the predictors and hence of the SSC indicators in a cross validation setting, pointing toward their general applicability for statistical downscaling (as developed and applied here) in the context of forecasting SSC variability. However, what we present here is only the first step and provides a benchmark for future assessments toward effective and operational use of decadal climate model output to forecast SSC variability. More work is clearly needed to better understand the physical mechanisms connecting SSC variability and large-scale teleconnections and to assess in more detail, for individual locations and seasons, the ability (or lack thereof) of the models to capture the relevant predictor variability.

In general, the ability to forecast SSC variability would allow quantification of the fluctuations of extreme sea levels around long-term MSL changes and hence support coastal planning and decision-making in the context of short- and medium-term coastal adaptation efforts, such as beach nourishment or building berms and dunes. The framework adopted here could also be used to explore long-term changes in SSC variability using outputs from uninitialized centennial Global Climate Model (GCM) runs but noting that the phasing of peaks would not be reproduced in these simulations.

Data Availability Statement

The hourly tide gauge data used to derive SSC indicators in R19 were collected from three different sources: University of Hawaii Sea Level Center (UHSLC) database, Global Extreme Sea Level Analysis (GESLA) database, and National Oceanic and Atmospheric Administration (NOAA) water level database. Climate indices were downloaded from the website of the Global Climate Observation System (GCOS) Working Group on Surface Pressure (WG-SP). We acknowledge the World Climate Research Program's Working Group on Coupled Modeling for making available their model outputs used in this study. NOAA's Geophysical Fluid Dynamics Laboratory (GFDL) decadal climate experiment (GFDL-CM21) datasets are accessible online through https://esgf-node.llnl.gov/search/cmip5/.

Acknowledgments

This study was supported by NOAA's Climate Program Office, Climate Monitoring Program, Award Number NA17OAR4310158. We thank Dr. Dipayan Chowdhury for his support in applying drift correction of initialized decadal climate model outputs.

References

Bromirski, P. D., Flick, R. E., & Cayan, D. R. (2003). Storminess variability along the California coast: 1858–2000. *Journal of Climate*, *16*(6), 982–993. https://doi.org/10.1175/1520-0442(2003)016<0982:SVATCC>2.0.CO;2

Bromirski, P. D., Flick, R. E., & Miller, A. J. (2017). Storm surge along the Pacific coast of North America. *Journal of Geophysical Research: Oceans*, *122*, 441–457. https://doi.org/10.1002/2016JC012178

Carson, M., Köhl, A., Stammer, D., Meyssignac, B., Church, J., Schröter, J., et al. (2017). Regional sea level variability and trends, 1960–2007: A comparison of sea level reconstructions and ocean syntheses. *Journal of Geophysical Research: Oceans*, *122*, 9068–9091. https://doi.org/10.1002/2017JC012992

Cayan, D. R., Bromirski, P. D., Hayhoe, K., Tyree, M., Dettinger, M. D., & Flick, R. E. (2008). Climate change projections of sea level extremes along the California coast. *Climatic Change*, *87*(S1), 57–73. https://doi.org/10.1007/s10584-007-9376-7

Choudhury, D., Mehrotra, R., Sharma, A., Sen Gupta, A., & Sivakumar, B. (2019). Effectiveness of CMIP5 decadal experiments for interannual rainfall prediction over Australia. *Water Resources Research*, *55*, 7400–7418. https://doi.org/10.1029/2018WR024462

Choudhury, D., Sen Gupta, A., Sharma, A., Mehrotra, R., & Sivakumar, B. (2017). An assessment of drift correction alternatives for CMIP5 decadal predictions. *Journal of Geophysical Research: Atmospheres*, *122*, 10,282–10,296. https://doi.org/10.1002/2017JD026900

Choudhury, D., Sharma, A., Sivakumar, B., Gupta, A. S., & Mehrotra, R. (2015). On the predictability of SSTA indices from CMIP5 decadal experiments. *Environmental Research Letters*, *10*(7), 074013. https://doi.org/10.1088/1748-9326/10/7/074013

Dangendorf, F., Calafat, M., Arns, A., Wahl, T., Haigh, I. D., & Jensen, J. (2014). Mean sea level variability in the North Sea: Processes and implications. *Journal of Geophysical Research: Oceans*, *119*(10), 6820–6841. https://doi.org/10.1002/2014JC009901

Dangendorf, S., Müller-Navarra, J., Jensen, F., Schenk, T. W., & Weisse, R. (2014). North Sea storminess from a novel storm surge record since AD 1843. *Journal of Climate*, *27*(10), 3582–3595. https://doi.org/10.1175/JCLI-D-13-00427.1

Daubechies, I. (1988). Orthonormal bases of compactly supported wavelets. *Communications on Pure and Applied Mathematics*, *41*(7), 909–996. https://doi.org/10.1002/cpa.3160410705

He, X., & Guan, H. (2013). Multiresolution analysis of precipitation teleconnections with large-scale climate signals: A case study in South Australia. *Water Resources Research*, *49*, 6995–7008. https://doi.org/10.1002/wrcr.20560

ICPO (2011). Data and bias correction for decadal climate predictions, *International CLIVAR Project Office Publication Series* (Rep., 5 pp).

Jiang, Z., Sharma, A., & Johnson, F. (2020). Refining predictor spectral representation using wavelet theory for improved natural system modeling. *Water Resources Research*, *56*, e2019WR026962. https://doi.org/10.1029/2019WR026962

Kennedy, A. J., Griffin, M. L., Morey, S. L., Smith, S. R., & O'Brien, J. J. (2007). Effects of El Niño-Southern Oscillation on sea level anomalies along the Gulf of Mexico coast. *Journal of Geophysical Research*, *112*, C05047. https://doi.org/10.1029/2006JC003904

Kharin, V., Boer, G., Merryfield, W., Scinocca, J., & Lee, W. S. (2012). Statistical adjustment of decadal predictions in a changing climate. *Geophysical Research Letters*, *39*, L19705. https://doi.org/10.1029/2012GL052647

Komar, P. D., Allan*, J. C., & Ruggiero, P. (2011). Sea level variations along the US Pacific Northwest coast: Tectonic and climate controls. *Journal of Coastal Research*, *27*(5), 808–823.

Kopp, R. E., Kemp, A. C., Bittermann, K., Horton, B. P., Donnelly, J. P., Gehrels, W. R., et al. (2016). Temperature-driven global sea-level variability in the Common Era. *Proceedings of the National Academy of Sciences USA*, *113*(11), E1434–E1441. https://doi.org/10.1073/pnas.1517056113

Mamalakis, A., Yu, J.-Y., Randerson, J. T., AghaKouchak, A., & Foufoula-Georgiou, E. (2018). A new interhemispheric teleconnection increases predictability of winter precipitation in southwestern US. *Nature Communications*, *9*(1), 1–10.

Marcos, M., Calafat, F. M., Berihuete, Á., & Dangendorf, S. (2015). Long-term variations in global sea level extremes. *Journal of Geophysical Research: Oceans*, *120*, 8115–8134. https://doi.org/10.1002/2015JC011173

Matei, D., Pohlmann, H., Jungclaus, J., Müller, W., Haak, H., & Marotzke, J. (2012). Two tales of initializing decadal climate prediction experiments with the ECHAM5/MPI-OM model. *Journal of Climate*, *25*(24), 8502–8523. https://doi.org/10.1175/JCLI-D-11-00633.1

Newey, W. K., & West, K. D. (1986). *A simple, positive semi-definite, heteroskedasticity and autocorrelation consistent covariance matrix, edited*. MA, USA: National Bureau of Economic Research Cambridge.

Park, J., Obeysekera, J., & Barnes, J. (2010). Temporal energy partitions of Florida extreme sea level events as a function of Atlantic Multidecadal Oscillation. *Ocean Science*, *6*(2), 587–593. https://doi.org/10.5194/os-6-587-2010

Park, J., Obeysekera, J., Irizarry-Ortiz, M., Barnes, J., & Park-Said, W. (2010). Climate links and variability of extreme sea-level events at Key West, Pensacola, and Mayport, Florida. *Journal of Waterway, Port, Coastal, and Ocean Engineering*, *136*(6), 350–356. https://doi.org/10.1061/(ASCE)WW.1943-5460.0000052

Rashid, M. M., & Beecham, S. (2019). Simulation of streamflow with statistically downscaled daily rainfall using a hybrid of wavelet and GAMLSS models. *Hydrological Sciences Journal*, *64*(11), 1327–1339. https://doi.org/10.1080/02626667.2019.1630742

Rashid, M. M., Beecham, S., & Chowdhury, R. K. (2015). Statistical downscaling of CMIP5 outputs for projecting future changes in rainfall in the Onkaparinga catchment. *Science of the Total Environment*, *530*, 171–182.

Rashid, M. M., Beecham, S., & Chowdhury, R. K. (2016). Statistical downscaling of rainfall: A non-stationary and multi-resolution approach. *Theoretical and Applied Climatology*, *124*(3–4), 919–933. https://doi.org/10.1007/s00704-015-1465-3

Rashid, M. M., Johnson, F., & Sharma, A. (2018). Identifying sustained drought anomalies in hydrological records: A wavelet approach. *Journal of Geophysical Research: Atmospheres*, *123*, 7416–7432. https://doi.org/10.1029/2018JD028455

Rashid, M. M., Wahl, T., Chambers, D. P., Calafat, F. M., & Sweet, W. V. (2019). An extreme sea level indicator for the contiguous United States coastline. *Scientific Data*, *6*(1), 1–14.

Sachindra, D., Huang, F., Barton, A., & Perera, B. (2014). Multi-model ensemble approach for statistically downscaling general circulation model outputs to precipitation. *Quarterly Journal of the Royal Meteorological Society*, *140*(681), 1161–1178. https://doi.org/10.1002/qj.2205

Salvi, K., Villarini, G., & Vecchi, G. A. (2017). High resolution decadal precipitation predictions over the continental United States for impacts assessment. *Journal of Hydrology*, *553*, 559–573. https://doi.org/10.1016/j.jhydrol.2017.07.043

Salvi, K., Villarini, G., Vecchi, G. A., & Ghosh, S. (2017). Decadal temperature predictions over the continental United States: Analysis and enhancement. *Climate Dynamics*, *49*(9–10), 3587–3604. https://doi.org/10.1007/s00382-017-3532-1

Saurral, R. I., García-Serrano, J., Doblas-Reyes, F. J., Díaz, L. B., & Vera, C. S. (2020). Decadal predictability and prediction skill of sea surface temperatures in the South Pacific region. *Climate Dynamics*, *54*, 3945–3958.

Serafin, K. A., & Ruggiero, P. (2014). Simulating extreme total water levels using a time-dependent, extreme value approach. *Journal of Geophysical Research: Oceans*, *119*, 6305–6329. https://doi.org/10.1002/2014JC010093

Smith, D., Eade, R., Scaife, A. A., Caron, L.-P., Danabasoglu, G., DelSole, T., et al. (2019). Robust skill of decadal climate predictions. *Npj Climate and Atmospheric Science*, *2*(1), 1–10.

Sweet, W. V., & Zervas, C. (2011). Cool-season sea level anomalies and storm surges along the US East Coast: Climatology and comparison with the 2009/10 El Niño. *Monthly Weather Review*, *139*(7), 2290–2299. https://doi.org/10.1175/MWR-D-10-05043.1

Talke, S. A., Orton, P., & Jay, D. A. (2014). Increasing storm tides in New York Harbor, 1844–2013. *Geophysical Research Letters*, *41*, 3149–3155. https://doi.org/10.1002/2014GL059574

Thompson, P. R., Mitchum, G. T., Vonesch, C., & Li, J. (2013). Variability of winter storminess in the eastern United States during the twentieth century from tide gauges. *Journal of Climate*, *26*(23), 9713–9726. https://doi.org/10.1175/JCLI-D-12-00561.1

Wahl, T., & Chambers, D. P. (2015). Evidence for multidecadal variability in US extreme sea level records. *Journal of Geophysical Research: Oceans*, *120*, 1527–1544. https://doi.org/10.1002/2014JC010443

Wahl, T., & Chambers, D. P. (2016). Climate controls multidecadal variability in US extreme sea level records. *Journal of Geophysical Research: Oceans*, *121*, 1274–1290. https://doi.org/10.1002/2015JC011057